Journal Name

ARTICLE

Nearly hollow Ru-Cu-MoO_2 octahedrons consisting of clusters and nanocrystals for high efficiency hydrogen evolution reaction

Received 00th January 20xx,
Accepted 00th January 20xx

DOI: 10.1039/x0xx00000x

www.rsc.org/

Qian Liu[a,b], Chengtian Zhang[a], Pengyan Wang[a], Ding Chen[a], Manjie Xiao[a], Lei Chen[a], Suli Liu[c], Jun Yu[a,b], Shichun Mu[a,b]*

Regular hollow catalysts have aroused increasing attention in electrocatalysis owing to large surface area, much more active centers and fast mass transfer. Nevertheless, the structure regulation of regular hollow catalysts, especially octahedrons, is scarcely reported. Herein, by developing a facile strategy, we successfully integrate Ru clusters, and Cu-MoO_2 nanocrystals into a fused nearly hollow Ru-Cu-MoO_2 octahedron encapsulated with carbon. Due to the synergic effect and the advantageous structure and composition, such a multiple-nanocomponent catalyst merely requires 22 and 48 mV overpotentials at a current density of 10 mA cm^{-2} for hydrogen evolution reaction (HER) in 1 M KOH and 0.5 M H_2SO_4 solutions, respectively. More importantly, in alkaline seawater, nearly hollow Ru-Cu-MoO_2 octahedrons also present remarkable HER activity (23 mV @ 10 mA cm^{-2}), indicating potential applications in hydrogen production from seawater electrolysis. Furthermore, the density functional theory (DFT) calculation results unveil that the excellent catalytic activity of Ru-Cu-MoO_2 is on account of its relatively low hydrogen adsorption Gibbs free energy (ΔG_{H^*}) and water adsorption energy. The present work provides a new approach to designing advanced Ru-based catalysts toward HER and beyond.

1. Introduction

Nowadays, the rapid exhaustion of fossil fuels and the accompanying severe environmental problem make it imperative to develop clean and renewable energy.[1, 2] Hydrogen energy, as a pollution-free secondary energy with high calorific value, has aroused worldwide attention. Among various hydrogen-production methods, the electrochemical water splitting is regarded as a prospect on account of its simplicity and environmentally friendly.[3, 4] Given that seawater accounts for 97% water resources on the earth, it is of great potential to produce hydrogen via direct electrolysis of inexhaustible seawater. However, cost-efficient and stable cathode catalysts are urgently demanded for hydrogen evolution reaction (HER).[5] Hitherto, platinum (Pt) is regarded as optimal catalyst for HER due to its appropriate hydrogen adsorption Gibbs free energy ($\triangle G_{H^*}$). Nevertheless, the scarce reserves and exorbitant price seriously restrict its industry-scale applications.[6, 7] In addition, it is well known that the reaction rate of hydrogen evolution in alkaline media is much lower than that in acidic media.[8, 9] However, industrial hydrogen production is predominantly based on alkaline electrolytic cells. In this respect, developing HER cathode catalysts in alkaline media with low-cost and admirable performance, is challenging but significant.

In recent decades, the HER properties of other less expensive Pt-group metals have been explored due to their similar electronic structure and chemical inertia to Pt.[10] Among them, Ru is considered as the most likely alternative for Pt catalysts in HER owing to the similar metal-hydrogen bond strength to Pt but a much lower price.[11-13] Ru-based catalysts can improve the intrinsic catalytic activity and expose more active sites through designing reasonable structures, selecting the suitable conductive carrier, and adjusting the electronic property.[14] In addition, molybdenum dioxide (MoO_2) and earth-abundant transition metals such as Ni, Fe and Cu have attracted wide attention in HER because of their high chemical stability and electrochemical activity.[15, 16] Moreover, as reported, heterogeneous or multiple-nanocomponent catalysts tend to exhibit better catalytic performance than single-phase catalysts. For instance, MoO_2-Ni heterostructure presents excellent HER activity.[17] However, compared with Pt catalysts, its electrochemical activity is still far from satisfactory. Thus, to reach remarkable Pt-like HER activity, rational design of Ru-based catalysts with transition metal-MoO_2 heterostructure is supposed.

Commonly, the performance of catalysts is determined by the synergy of the structure and chemical composition.[18] On the one hand, regular hollow nanostructures possess large

[a] State Key Laboratory of Advanced Technology for Materials Synthesis and Processing, Wuhan University of Technology, Wuhan 430070, China.,
[b] Foshan Xianhu Laboratory of the Advanced Energy Science and Technology Guangdong Laboratory, Xianhu hydrogen Valley, Foshan 528200, China.
[c] Key Laboratory of Advanced Functional Materials of Nanjing, Nanjing Xiaozhuang University, Nanjing 211171, Jiangsu, China
* Corresponding author E-mail: msc@whut.edu.cn; niuniu_410@126.com

specific surface area, which could provide abundant surface active sites, and then diminish the dosage of noble metals. On the other hand, regular hollow materials can reduce the mass transfer distance.[19-21] Therefore, regular hollow nanostructures catch great attention in the electrochemical energy conversion and storage fileds.[22] For example, by mean of a templated-assisted assembly method, Lou's group synthesized M-MoS_3(M=Co, Ni) hollow structures for efficient HER processes.[23] In addition, other methods, such as chemical etching,[24] galvanic replacement[25] and Kerkendal diffusion[26] were also employed to construct such hollow nanostructures. Although great achievements have been achieved so far, it is still a difficult task to design and realize controllable hollow nanostructures in a simple way.

Herein, NENU-5, with rich copper ions[27, 28], is selected as the precursor. Then a simple ion exchange between Cu^{2+} and Ru^{3+} happens to synthesize Ru-Cu-MoO_2 multiple-nanocomponent catalysts consisting of nearly hollow octahedrons, in which Ru and Cu-MoO_2 are presented as cluster and nanocrystal, respectively. As expected, Ru-Cu-MoO_2 performs distinguished HER catalytic activity in both alkaline and acidic conditions. In addition, our theoretical calculation results further evidence that Ru-Cu-MoO_2 owns an optimal ΔG_{H^*} value and a water adsorption energy, thus reducing the HER kinetic barrier.

2. Experimental section

Preparation of NENU-5

NENU-5 is a kind of MOF with large specific surface area and high porosity. The detailed synthesis scheme can be found in supporting information.

Preparation of Ru-NENU-5

200 mg NENU-5 was added into 80 mL mixed solution (ethanol: water = 1:1), and then homogenized by ultrasonic dispersion. After that, a $RuCl_3$ ethanol solution (1.25, 2.5, 3.75 and 5 mL) was injected into it. The mixture was stirred at 70 ℃ for 24, 48 or 96 h. After centrifugation, washing and drying, a gray-green product was gained.

Preparation of Cu-MoO_2 and Ru-Cu-MoO_2

NENU-5 and Ru-NENU-5 powders were heated to 600 ℃ at a rate of 2 ℃/min and kept for 3 h. When naturally cooled down, Cu-MoO_2, Ru-Cu-MoO_2-24h, Ru-Cu-MoO_2-48h and Ru-Cu-MoO_2-96h were obtained. The entire annealing process was completed in an argon atmosphere.

3. Results and discussion

Synthesis and structure of nearly hollow Ru-Cu-MoO_2 octahedrons

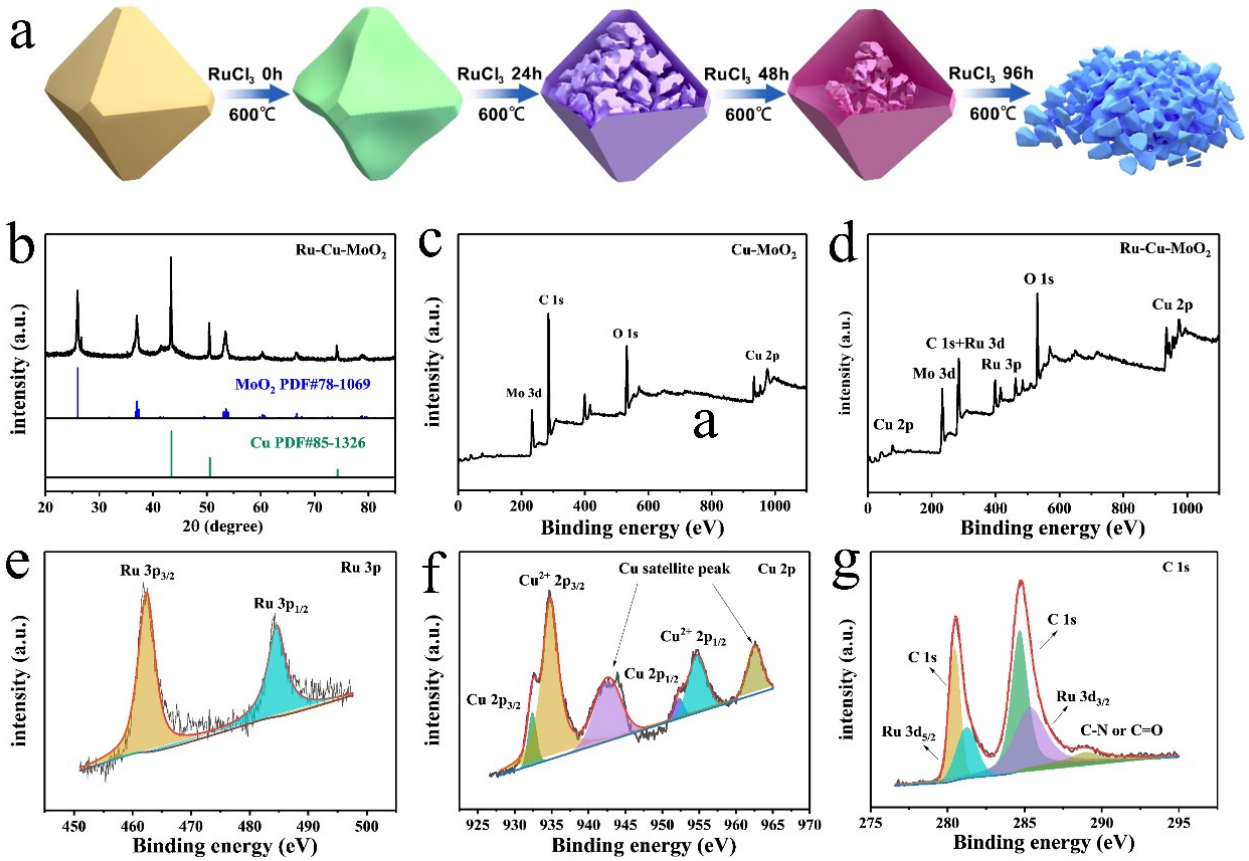

Figure 1. (a) Schematic synthesis Procedure for Ru-Cu-MoO_2. (b) XRD pattern of Ru-Cu-MoO_2. (c) XPS Survey spectrum of Cu-MoO_2. (d) Survey spectrum of Ru-Cu-MoO_2. (e) Ru 3p, (f) Cu 2p and (g) C 1s.

Journal Name

ARTICLE

The synthetic route of Ru-Cu-MoO_2 hollow octahedrons is displayed in **Figure 1a**. First of all, NENU-5 was formed by a room temperature co-precipitation method. Scanning electron microscope (SEM) image illustrates that NENU-5 (**Figure S1a**) is of truncated octahedrons with uniform size distribution of 800 nm. Subsequently, using NENU-5 as the precursor, the intermediate Ru-NENU-5 was synthesized by virtue of a simple ion exchange method. It can be easily discovered that Ru-NENU-5 (**Figure S1b**) basically retains the octahedral structure and size equivalent to NENU-5. However, after reaction with $RuCl_3$, part of the surface of NENU-5 was etched and the surface became rough. X-ray diffraction (XRD) patterns elucidate that both NENU-5 and Ru-NENU-5 have good crystallinity, and the periodic crystal structure of Ru-NENU-5 still remains intact after the ion exchange reaction (**Figure S2a** and **b**). Finally, NENU-5 and Ru-NENU-5 were annealed at 600 °C, respectively. After high temperature annealing of NENU-5, sharp characteristic peaks of Cu and MoO_2 appear in the XRD pattern (**Figure S2c**), indicating that Cu-MoO_2 was formed by thermal reduction. The XRD pattern of Ru-Cu-MoO_2-48h (**Figure 1b**) displays strong peaks of Cu and MoO_2, which come from the thermal reduction of the precursor. Among them, the peaks at 43.3, 50.4, and 74.1° are assigned to the (111), (200) and (220) crystal planes of Cu, respectively. While the four peaks at 26.0, 36.9, 53.5, and 60.0° match severally with the (011), (-112), (220) and (031) crystal faces of MoO_2. Significantly, the characteristic peak of Ru does not appear in the XRD pattern, evidencing that Ru might be in cluster or other states.

In addition, from X-ray photoelectron spectroscopy (XPS) spectra of Cu-MoO_2 and Ru-Cu-MoO_2 (**Figure 1c** and **d**), it not only shows that the Ru-Cu-MoO_2 catalyst is composed of Ru, Cu, Mo, C and O elements, but also confirms the ion exchange between Ru^{3+} and Cu^{2+} and the successful modification of Ru^{3+} on NENU-5. In **Figure 1e**, two peaks situated at 462.4 and 484.6 eV, correspond to the zero-valence state of Ru $3p_{3/2}$ and Ru $3p_{1/2}$, respectively. As **Figure 1f** shows, the peaks at 932.4 and 952.3 eV belong to Cu, while the peaks at 934.8 and 954.7 eV indicate the presence of Cu^{2+}. The appearance of Cu^{2+} may be related to partial oxidation of the catalyst exposed to air. In the XPS spectrum of Mo (**Figure S3**), the peaks at 229.7 and 232.4 eV should stem from MoO_2 formed after high temperature pyrolysis. While the peaks at the 232.0 and 235.5 eV derive from MoO_3, due to the surface oxidation of MoO_2 exposed to the air.[29, 30] The peaks of the Ru 3d orbit also exist in the XPS spectrum of C 1s (**Figure 1g**), consistent with previous reports, which also proves the successful modification of Ru on NENU-5 from another perspective.[31]

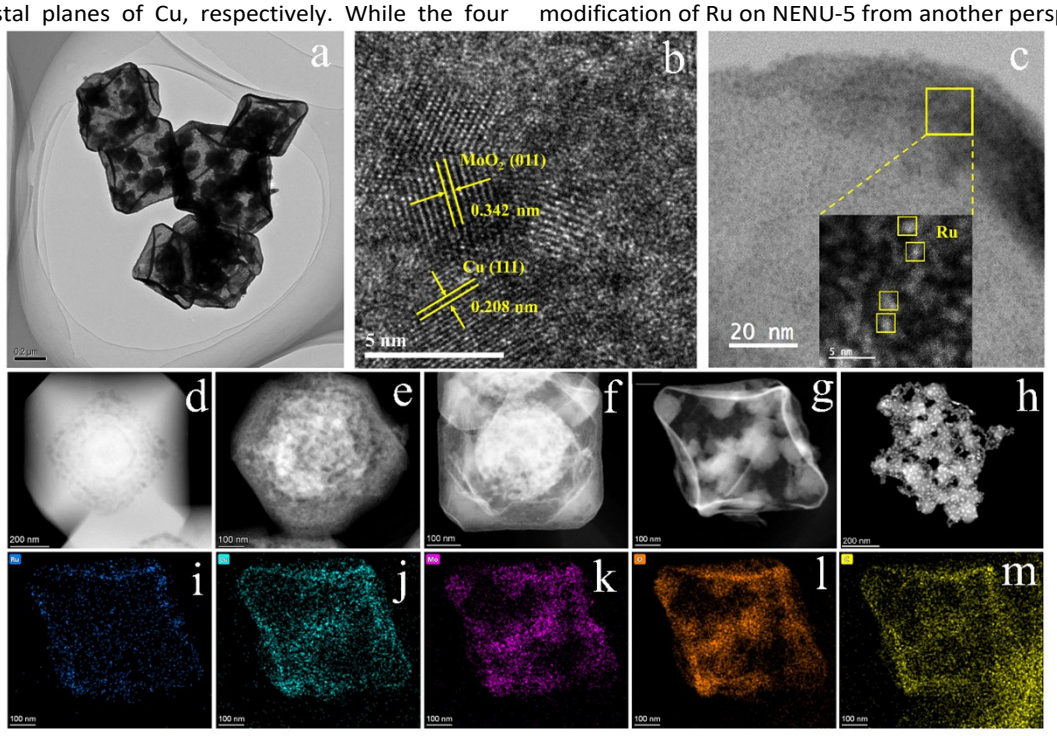

Figure 2. (a) TEM, (b) HRTEM and (c) STEM image of Ru-Cu-MoO_2-48h. (d) HADDF-STEM image of NENU-5, (e) Cu-MoO_2, (f) Ru-Cu-MoO_2-24h, (g) Ru-Cu-MoO_2-48h. (h) Ru-Cu-MoO_2-96h. (i-m) EDX elemental mapping of Ru, Cu, Mo, O and C of Ru-Cu-MoO_2-48h.

Journal Name

ARTICLE

Figure S4 demonstrates that Ru-Cu-MoO_2 has a slightly reduced size of 600 nm compared to Ru-NENU-5, but still maintains the octahedral shape. Transmission electron microscope (TEM) proves that the interior of the catalyst is mostly hollow but filled with multi-cores (**Figure 2a**). High-resolution TEM (HRTEM) image of the catalyst in **Figure 2b** reveals the presence of Cu and MoO_2 nanocrystals. Among the lattice fringes, the lattice spacing of 0.208 and 0.342 nm corresponds to the (111) crystal plane of Cu and (011) crystal plane of MoO_2, respectively. This result coincides with previous XRD analysis results. In addition, the deeper observation via high angle annular dark field STEM (HAADF-STEM) unveils the existence of Ru as clusters (**Figure 2c**). The energy-dispersive X-ray spectroscopy (EDS) spectrum (**Figure 2j-m**) further clarifies that the Cu, Mo, O, and C elements are uniformly distributed throughout the solid part of the octahedron including predominant shells and multi-cores inside. It's worth noting that Ru is distributed on such solid surfaces (**Figure 2i** and **S5**), which can promote the HER process by offering more active sites.[32, 33]

To explore the formation and evolution of the hollow nanostructure for Ru-Cu-MoO_2 octahedrons, we investigated the effect of the reaction time on these processes. **Figure 2d** manifests that NENU-5 is a solid structure. Similarly, Cu-MoO_2 formed by means of high temperature annealing of NENU-5 has a porous solid nanostructure as well (**Figure 2e**). As exhibited in **Figure 2f**, after 24 h, the outer ring of Ru-Cu-MoO_2 begins to change from complete solid to hollow. After 48 h, the solid is almost depleted and the hollow structure inside the octahedron becomes extremely apparent (**Figure 2g**). However, the octahedral structure is completely collapsed when the reaction time reaches 96 h (**Figure 2h** and **S6**). This structural evolution marks that $RuCl_3$ could destroy the structure of NENU-5 after a 96 h reaction, making it unable to hold its original form. The formation mechanism of the nearly hollow Ru-Cu-MoO_2 octahedron can be described as follows. After adding $RuCl_3$ to NENU-5, Ru^{3+} would swap with Cu^{2+} and occupy the Cu^{2+} sites in NENU-5. Subsequently, Ru^{3+} starts to slowly etch the surface of NENU-5 from outside to inside. With the reaction, Ru^{3+} gradually enters the octahedron, destroying the original solid structure of NENU-5. Then, after high-temperature annealing, it shrinks and crystallizes to form hollow nanoparticles. Nevertheless, if the reaction time is too long, most of Cu^{2+} in NENU-5 would be replaced by Ru^{3+}, causing the octahedral structure to collapse. In addition, the content of Ru, Cu and Mo of Ru-Cu-MoO_2-24h, Ru-Cu-MoO_2-48h and Ru-Cu-MoO_2-96h was measured by inductively coupled plasma optical emission spectrometry (ICP-OES). As shown in **Table S1**, the content of Ru in Ru-Cu-MoO_2-24h, Ru-Cu-MoO_2-48h and Ru-Cu-MoO_2-96h is 10.69, 14.39 and 45.71 wt%, respectively, indicating the content of Ru increases with the reaction time. The longer the reaction time is, the more sufficient the ion exchange is, which leads to the increased Ru content.

HER performance of Ru-Cu-MoO_2 nearly hollow octahedrons

First, a three-electrode system was utilized to measure the HER performance of the catalyst at different ratios. **Figure S7** hints that, when the mass ratio of NENU-5 to $RuCl_3$ is 200 to 50 in both alkaline and acid conditions, the catalyst provides the best HER performance. Adjacently, we probed the HER performance of the catalyst at different reaction times under the optimal ratio. The linear sweep voltammetry (LSV) polarization curve in **Figure 3a** elucidates that Cu-MoO_2 has almost no catalytic activity. Impressively, when Ru^{3+} was introduced, Ru-Cu-MoO_2 shows advantageous catalytic activity. Specifically, the overpotential of Ru-Cu-MoO_2-48h at the current density of 10 mA cm^{-2} is merely 22 mV, exceeding the activity of commercial Pt/C (36 mV). Compared with the optimal sample, to reach the same current density, Ru-Cu-MoO_2-24h and Ru-Cu-MoO_2-96h require 38 and 176 mV overpotential, respectively.

To better explore the HER kinetics of Ru-Cu-MoO_2, the Tafel curve was plotted. **Figure 3b** and **c** present the Tafel slope of 35 mV dec^{-1} for Ru-Cu-MoO_2-48h, smaller than that of Ru-Cu-MoO_2-24h (69 mV dec^{-1}), Ru-Cu-MoO_2-96h (148 mV dec^{-1}) and close to Pt/C (34 mV dec^{-1}). This testifies that Ru-Cu-MoO_2-48h owns rapid electron transfer rate and HER kinetics. In addition, the double layer capacitance (C_{dl}) of the catalyst was acquired by cyclic voltammetry (CV) test in the non-Faraday current region (**Figure S8-10**). The C_{dl} value (**Figure 3d**) of Ru-Cu-MoO_2-48h is 49.6 mF cm^{-2}, greater than Ru-Cu-MoO_2-24h (24.8 mF cm^{-2}), Ru-Cu-MoO_2-96h (21.2 mF cm^{-2}) and Cu-MoO_2 (4.91 mF cm^{-2}). This result manifests that Ru-Cu-MoO_2-48h owns a larger electrochemical active area. Moreover, the electrochemical impedance (**Figure 3e**) of different samples was measured. Ru-Cu-MoO_2-48h shows minimal charge transfer resistance (R_{ct}). In summary, Ru-Cu-MoO_2-48h owns tremendous HER activity as a result of its high intrinsic catalytic activity with enormous electrochemical active area and active sites, as well as fast charge transfer ability.

Because the stability determines whether HER catalyst can be used for a long time, the hydrogen evolution activity after 1000, 2000 and 3000 cycles was examined via CV test. As shown in **Figure 3f**, after 3000 CV cycles, the polarization curve of Ru-Cu-MoO_2-48h basically sustains the original activity. Besides, from **Figure S11a**, we discover that the current density remains basically unchanged at 10 mA cm^{-2} within 50 h.

By contrast, the stability test of commercial Pt/C catalysts was also performed (**Figure S12**). Obviously, the current density of Pt/C decreases continuously, which proves the better stability of Ru-Cu-MoO_2 than that of Pt/C. The CV and chronoamperometry test jointly evidence that Ru-Cu-MoO_2 does own good HER stability under alkaline conditions. XPS was used to explore the catalyst after test. By comparing the XPS spectra of Ru, Cu and Mo before and after 3000 accelerated CV cycling test for HER (**Figure S13**), the change in peaks of the Ru-Cu-MoO_2-48h catalyst is almost negligible, which proves its excellent stability.

In acidic solutions, when Ru-Cu-MoO_2-48h reaches a current density of 10 mA cm^{-2}, the overpotential is 48 mV (**Figure 3g**) and the corresponding Tafel slope is 60 mV dec^{-1} (**Figure 3h**). **Figure S14a** and **b** prove that Ru-Cu-MoO_2-48h also has a larger electrochemical active surface area and smaller R_{ct}. Minor changes in LSV curves after 3000 CV cycles (**Figure 3i**) and i-t curves (**Figure S11b**) evidence the good durability of the catalyst under acidic conditions. Additionally, the HER activity of Ru-Cu-MoO_2 is also advantageous compared with other Ruthenium-based catalysts reported under alkaline conditions (**Table S2**). Given the outstanding HER performance of Ru-Cu-MoO_2 in alkaline and acidic solutions, we tried to explore its catalytic activity in neutral solutions. However, Ru-Cu-MoO_2 needs 133 mV to drive the current density of 10 mA cm^{-2}, which is worse than Pt/C (**Figure S15**) and other advanced catalysts as reported.[34-36]

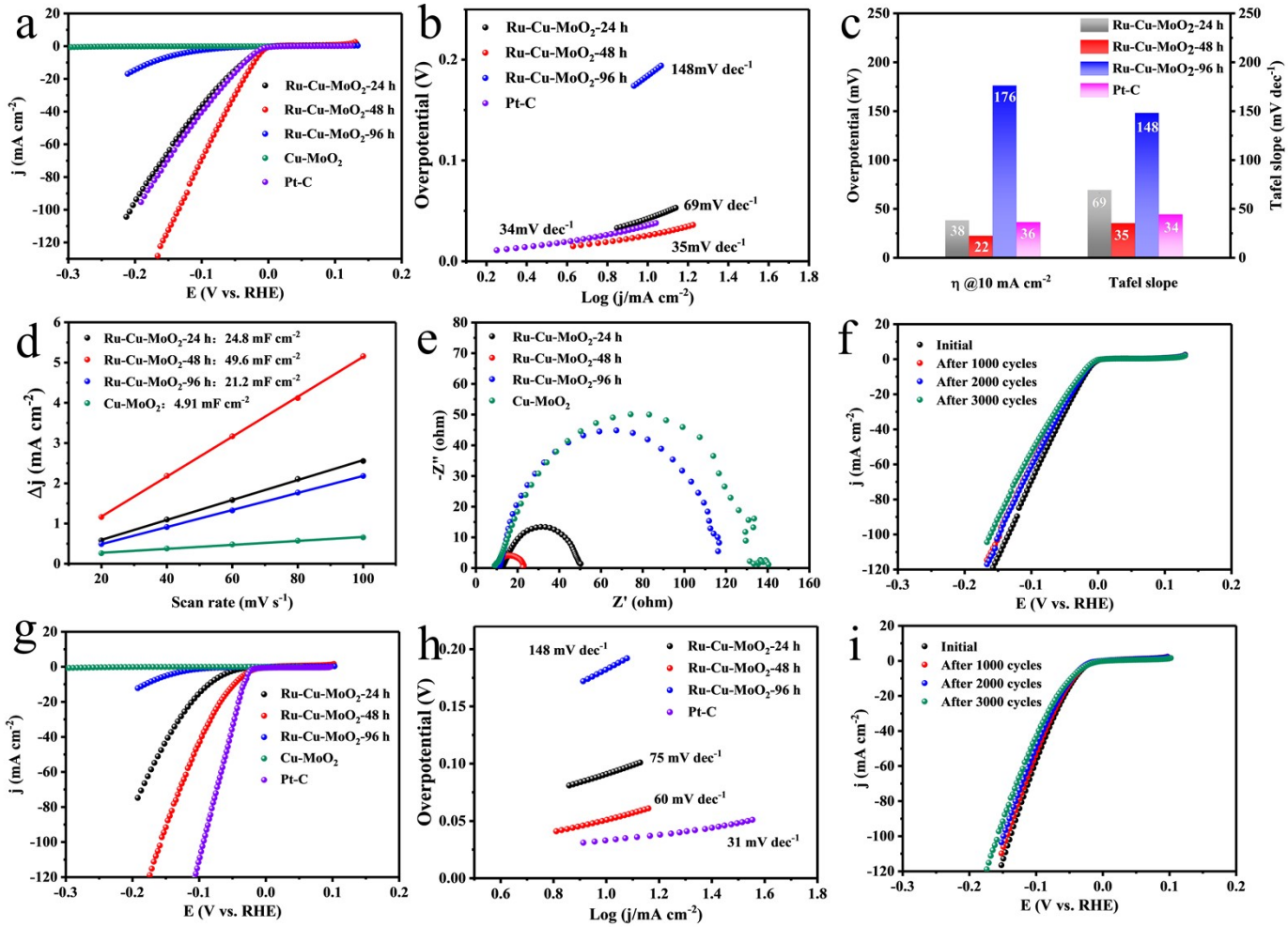

Figure 3. LSV curves in (a) 1 M KOH and (g) 0.5 M H_2SO_4. Corresponding Tafel slopes in (b) 1 M KOH and (h) 0.5 M H_2SO_4. (c) Overpotentials of the catalysts at 10 mA cm^{-2} and Tafel slopes in 1 M KOH. (d) C_{dl} in 1 M KOH. (e) Nyquist plots in 1 M KOH. LSV curves for Ru-Cu-MoO_2 after 1000, 2000 and 3000 cycles in (f) 1 M KOH and (i) 0.5 M H_2SO_4.

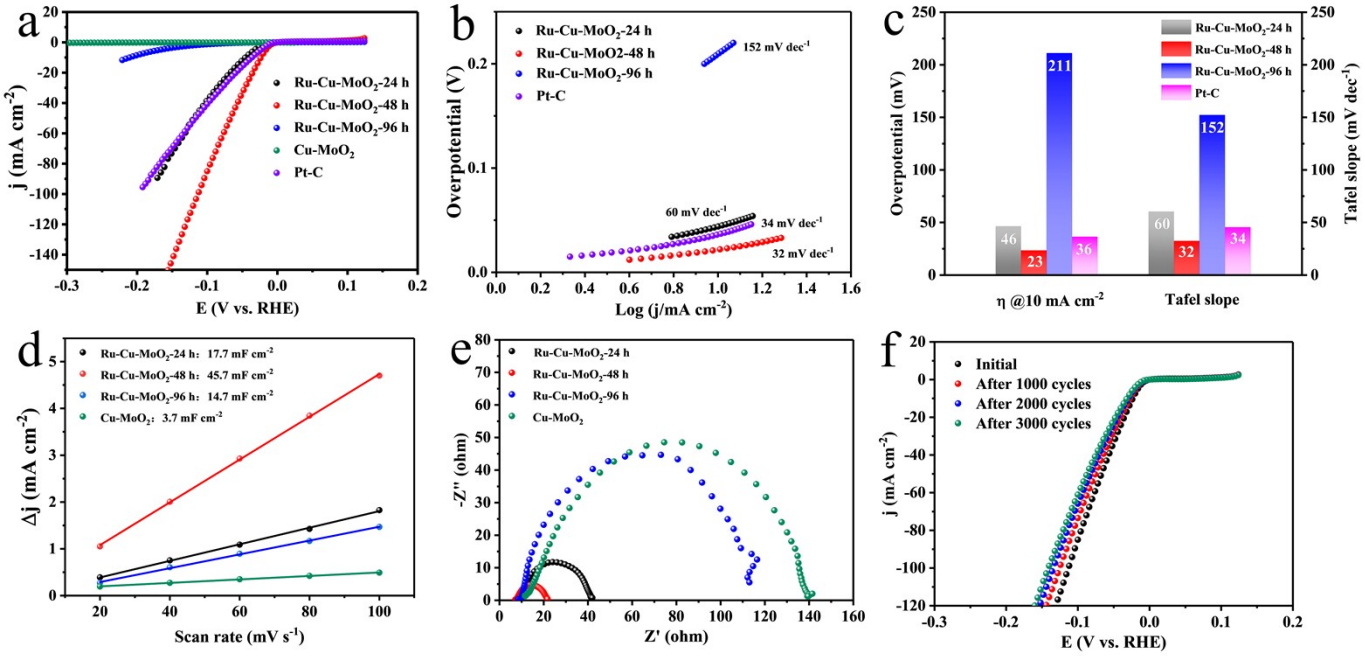

Figure 4. HER performance of Ru-Cu-MoO_2 in seawater media (pH=14). (a) LSV curves (b) Tafel slopes (c) Overpotentials of the catalysts at 10 mA cm^{-2} and Tafel slopes. (d) C_{dl} (e) Nyquist plots. (f) LSV curves for Ru-Cu-MoO_2 after 1000, 2000 and 3000 cycles.

Considering the splendid HER behavior of Ru-Cu-MoO_2 in alkaline solutions and abundant seawater resources, the catalytic activity of Ru-Cu–MoO_2 in alkaline seawater was inspected. **Figure 4a** manifests that Ru-Cu–MoO_2-48h merely needs 23 mV to reach a current density of 10 mA cm^{-2} in seawater media. **Figure 4b** and **c** show that the Tafel slope is 32 mV dec^{-1}, lower than commercial Pt/C (34 mV dec^{-1}). Compared with other samples, it has the largest C_{dl} (49.6 mF cm^{-2}) and the minimum R_{ct} (**Figure 4d** and **e**). Similar to the case in 1 M KOH solutions, Ru-Cu–MoO_2 also presents satisfactory stability in alkaline seawater (**Figure 4f** and **S11c**). These results attest that Ru-Cu-MoO_2-48h has outstanding HER catalytic activity and stability in alkaline seawater as well, indicating it may be applied to hydrogen production in seawater media under alkaline conditions.

Overall, these consequences verify that Ru-Cu-MoO_2 is equipped with wonderful catalytic activity and durability for HER in acidic, alkaline, and seawater media.

Water splitting performance in alkaline and seawater

In consideration of the terrific HER catalytic activity in 1 M KOH, the overall water splitting was further investigated by employing Ru-Cu-MoO_2 and commercial RuO_2 as the cathode and the anode. As benchmark, the electrolyzer with commercial Pt/C and RuO_2 was assembled. For the electrolyzer with Ru-Cu-MoO_2/RuO_2 electrodes, the overpotentials of 1.529 and 1.598 V are required to drive current densities of 10 mA cm^{-2} and 20 mA cm^{-2}, respectively, while 1.537 and 1.609 V separately for that with commercial Pt-C/RuO_2 electrodes (**Figure 5a**). In addition, **Figure 5b** illustrates that Ru-Cu-MoO_2/RuO_2 electrodes can maintain electrolytic stability within 25 h. These results indicate that Ru-Cu-MoO_2/RuO_2 possesses an admirable overall water splitting performance.

During the electrolysis process in alkaline solutions and seawater, hydrogen and oxygen produced by Ru-Cu-MoO_2/RuO_2 in 1M KOH and seawater media were collected (**Video S1 and S2**). As shown in the **Figure 5c** and **d**, we adopted drainage to collect hydrogen and oxygen. The volume ratio of hydrogen and oxygen released by the device in the media of 1 M KOH and seawater is approximately 2:1 (**Figure 5e**). In addition, the hydrogen yield of Ru-Cu-MoO_2 was tested (**Figure S16**) and the ratio is 97.1%, very close to100%. This proves that the Faraday efficiency of Ru-Cu-MoO_2 for water electrolysis is almost 100%.

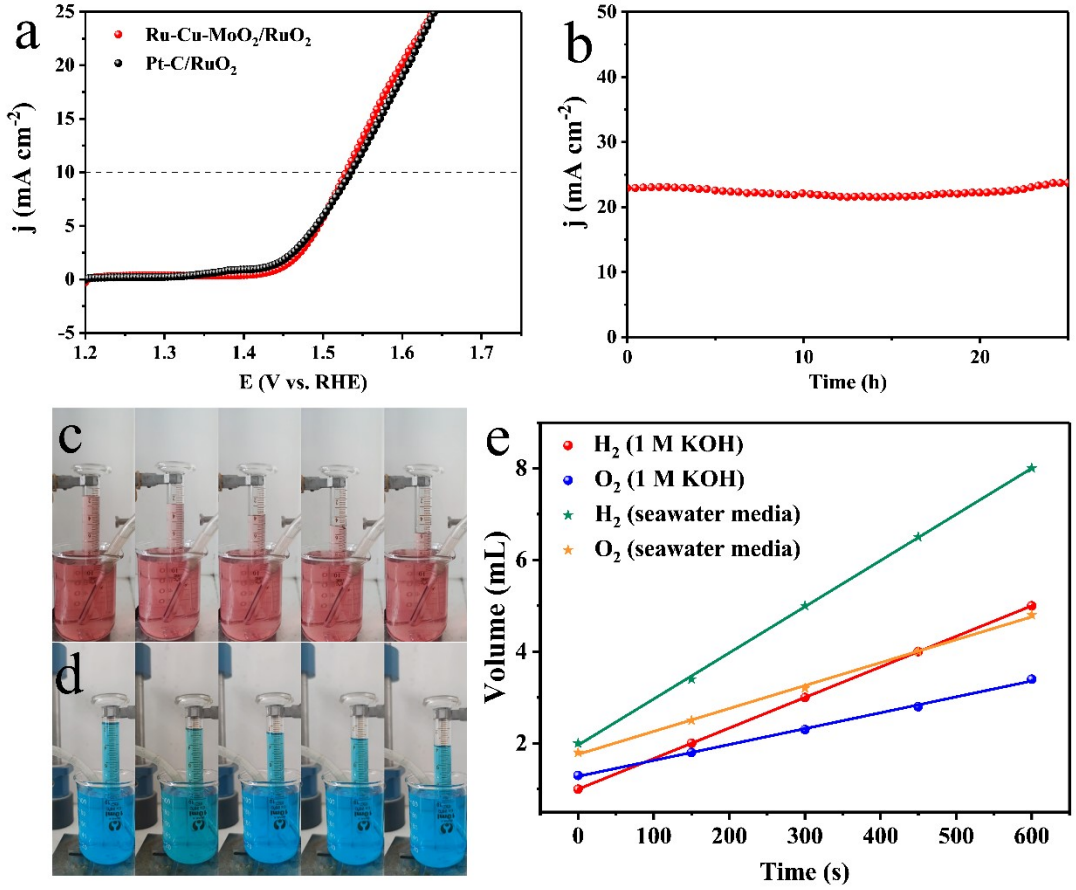

Figure 5. (a) LSV curves of Ru-Cu-MoO_2/RuO_2. (b) Time-reliant current density curve for Ru-Cu-MoO_2/RuO_2. (c) and (d) Optical images of produced H_2 and O_2 in 1 M KOH. (e) Graph of the total amount of O_2 and H_2 produced over time in 1 M KOH and seawater.

Theoretical calculation analysis

The catalytic mechanism of Ru-Cu-MoO_2 can be further explained by density functional theory (DFT). To keep up with the results in HRTEM, the most suitable (111) and (011) crystal planes were chosen for Cu and MoO_2, respectively. Corresponding theoretical models in DFT calculations are displayed in **Figure 6 a, b** and **S17**. To investigate the impact on Ru modification to the electrical conductivity, the density of states (DOS) of Cu-MoO_2 and Ru-Cu-MoO_2 were calculated. The value of Ru-Cu-MoO_2 is significantly larger than that of Cu-MoO_2 at the Fermi level (**Figure 6c**), suggesting that Ru-Cu-MoO_2 has a higher electrical conductivity. To acquire the hydrogen adsorption Gibbs free energy (ΔG_{H*}), the models of Cu, MoO_2, Cu-MoO_2 and Ru-Cu-MoO_2 adsorbed hydrogen atom were constructed (**Figure S18**). The ΔG_{H*} value is one of the most important criteria for evaluating HER catalyst, and the closer its value is to 0, the more favorable it is for hydrogen adsorption and desorption.[37, 38] Based on the calculation data in **Figure 6d**, the ΔG_{H*} value of Ru-Cu-MoO_2 and Cu-MoO_2 is -0.08 and 0.56 eV, respectively. It is elucidated that the surface contact between *H and Cu-MoO_2 is weak, leading to *H desorption easily from the catalyst. After the introduction of Ru, the ΔG_{H*} value of Cu-MoO_2 is extremely close to 0, indicating low kinetic barrier and good catalytic activity for HER. The lack of H^+ required for HER in alkaline solutions leads to an additional water molecular dissociation step in the Volmer reaction, so the water adsorption energy (ΔEH_2O) was also investigated (**Figure 6e**). Consistent with the results of ΔG_{H*}, Ru-Cu-MoO_2 exhibits the lowest ΔEH_2O value (-0.95 eV), proving that the binding strength of H_2O with Ru-Cu-MoO_2 is most appropriate compared with Cu, MoO_2 and Cu-MoO_2. The above DFT results demonstrate that the fusion of Ru into Cu-MoO_2 is conducive to improving electrical conductivity and optimizing the ΔG_{H*} and ΔE_{H2O}, thereby promoting the HER.

Journal Name

ARTICLE

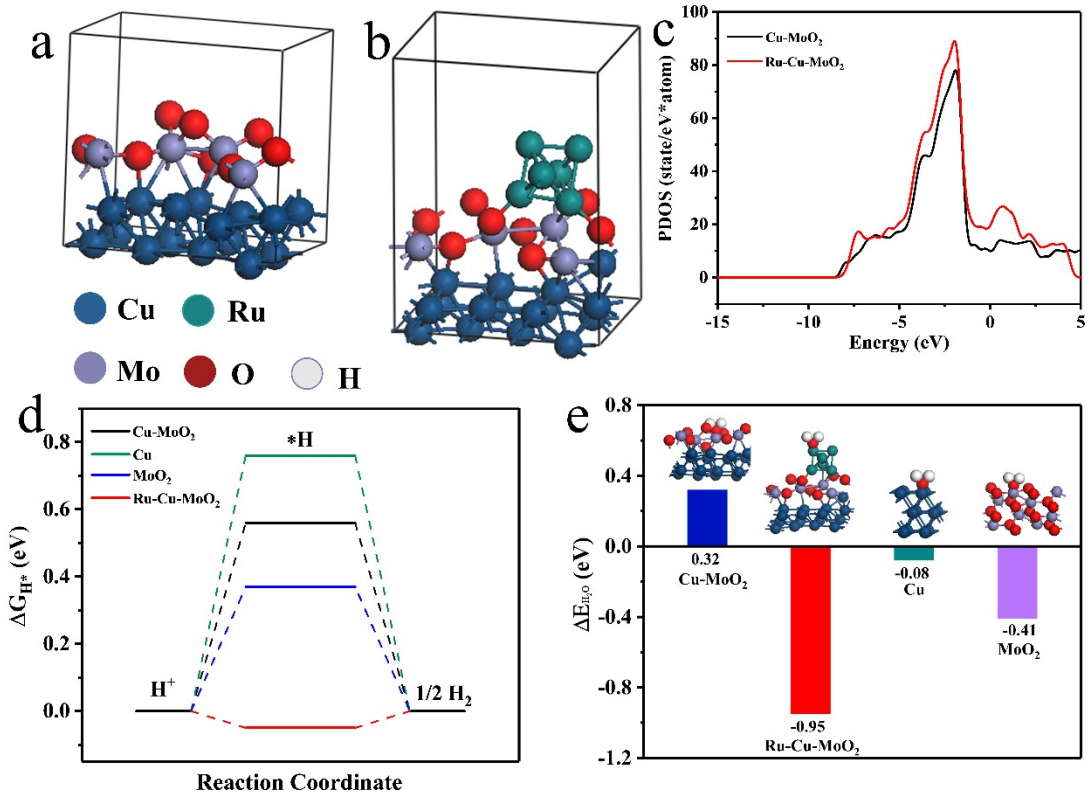

Figure 6. Structure models of (a) Cu-MoO_2 and (b) Ru-Cu-MoO_2. (c) The calculated DOS results of Cu-MoO_2 and Ru-Cu-MoO_2. (d) Free energy diagram and (e) water adsorption energies of Cu, MoO_2, Cu-MoO_2 and Ru-Cu-MoO_2.

All in all, the nearly hollow Ru-Cu-MoO_2 octahedron can provide the following advantages: First, the unique hollow structure with multi-cores makes full use of interior space of the hollow catalyst and allows Ru-Cu-MoO_2 with a large specific surface area and abundant active sites. Second, there are many voids inside the hollow octahedron, conducive to the mass transfer in the HER process. Besides, the large number of surfaces make most of Ru resident in the octahedral structure, which enhances the catalytic activity and utilization rate of Ru. Moreover, due to the synergic effect of Ru, Cu and MoO_2, the ΔG_{H^*} value of Ru-Cu-MoO_2 approaches to 0, meaning the fast HER kinetics. Finally, the MOF-derived carbon material as encapsulated layer has prominent electrical conductivity and can effectively avoid the agglomeration and corrosion/oxidation of metal moieties. On account of the above advantages, Ru-Cu-MoO_2 exhibits salient HER properties in alkaline, acidic and seawater.

4. Conclusions

In summary, with NENU-5 as the precursor, we synthesized nearly hollow Ru-Cu-MoO_2 octahedrons by a simple cation exchange method. The unique hollow nanostructure of the catalyst makes it possess outstanding HER properties. Indeed, to deliver a current density of 10 mA cm^{-2} under alkaline conditions, acidic and alkaline seawater conditions, it only needs overpotentials of 22, 48 and 23 mV, respectively. Additionally, the voltage of water splitting at 10 mA cm^{-2} for Ru-Cu-MoO_2/RuO_2 is 1.529 V, with nearly 100% Faraday efficiency and excellent electrochemical stability. The DFT calculation further unveils that the remarkable HER activity of Ru-Cu-MoO_2 comes from the ΔG_{H^*} value very close to zero and the appropriate water adsorption energy. Undoubtedly, this offers a novel idea for the catalyst design with high efficiency hydrogen production from water electrolysis.

Conflicts of interest

There are no conflicts to declare.

Acknowledgements

This work was supported by the National Natural Science Foundation of China (Grant No. 22075223, 22179104), and the State Key Laboratory of Advanced Technology for Materials Synthesis and Processing (Wuhan University of Technology) (2021-ZD-4), and Fundamental Research Funds for the Central Universities.

Notes and references

1. S.-Q. Liu, H.-R. Wen, G. Ying, Y.-W. Zhu, X.-Z. Fu, R. Sun and C.-P. Wong, *Nano Energy*, 2018, **44**, 7-14.
2. H. Zhou, Y. Wang, R. He, F. Yu, J. Sun, F. Wang, Y. Lan, Z. Ren and S. Chen, *Nano Energy*, 2016, **20**, 29-36.
3. X. Xiao, X. Wang, X. Jiang, S. Song, D. Huang, L. Yu, Y. Zhang, S. Chen, M. Wang, Y. Shen and Z. Ren, *Small Methods*, 2020, **4**, 1900653.
4. J. Yu, W.-J. Li, H. Zhang, F. Zhou, R. Li, C.-Y. Xu, L. Zhou, H. Zhong and J. Wang, *Nano Energy*, 2019, **57**, 222-229.
5. J. Zhu, L. Hu, P. Zhao, L. Y. S. Lee and K. Y. Wong, *Chem. Rev.*, 2020, **120**, 851-918.
6. H. Liao, Y. Sun, C. Dai, Y. Du, S. Xi, F. Liu, L. Yu, Z. Yang, Y. Hou, A. C. Fisher, S. Li and Z. J. Xu, *Nano Energy*, 2018, **50**, 273-280.
7. X. Cao, Y. Han, C. Gao, Y. Xu, X. Huang, M. Willander and N. Wang, *Nano Energy*, 2014, **9**, 301-308.
8. S. Ye, F. Luo, T. Xu, P. Zhang, H. Shi, S. Qin, J. Wu, C. He, X. Ouyang, Q. Zhang, J. Liu and X. Sun, *Nano Energy*, 2020, **68**, 104301.
9. K. Wu, K. Sun, S. Liu, W.-C. Cheong, Z. Chen, C. Zhang, Y. Pan, Y. Cheng, Z. Zhuang, X. Wei, Y. Wang, L. Zheng, Q. Zhang, D. Wang, Q. Peng, C. Chen and Y. Li, *Nano Energy*, 2021, **80**, 105467.
10. S. Yuan, Z. Pu, H. Zhou, J. Yu, I. S. Amiinu, J. Zhu, Q. Liang, J. Yang, D. He, Z. Hu, G. Van Tendeloo and S. Mu, *Nano Energy*, 2019, **59**, 472-480.
11. Q. He, D. Tian, H. Jiang, D. Cao, S. Wei, D. Liu, P. Song, Y. Lin and L. Song, *Adv. Mater.*, 2020, **32**, 1906972.
12. Z. Peng, H. Wang, L. Zhou, Y. Wang, J. Gao, G. Liu, S. A. T. Redfern, X. Feng, S. Lu, B. Li and Z. Liu, *J. Mater. Chem. A*, 2019, **7**, 6676-6685.
13. Z. Liu, X. Yang, G. Hu and L. Feng, *ACS Sustain. Chem. Eng.*, 2020, **8**, 9136-9144.
14. W. Luo, Y. Wang and C. Cheng, *Mater. Today Phys.*, 2020, **15**, 100274.
15. P. Jiang, Y. Yang, R. Shi, G. Xia, J. Chen, J. Su and Q. Chen, *J. Mater. Chem. A*, 2017, **5**, 5475-5485.
16. G. Yang, Y. Jiao, H. Yan, Y. Xie, A. Wu, X. Dong, D. Guo, C. Tian and H. Fu, *Adv. Mater,*. 2020, **32**, 2000455.
17. X. Liu, K. Ni, C. Niu, R. Guo, W. Xi, Z. Wang, J. Meng, J. Li, Y. Zhu, P. Wu, Q. Li, J. Luo, X. Wu and L. Mai, *ACS Catal.*, 2019, **9**, 2275-2285.
18. Z. X. Cai, Z. L. Wang, J. Kim and Y. Yamauchi, *Adv. Mater.*, 2019, **31**, 1804903.
19. L. Yu, J. F. Yang, B. Y. Guan, Y. Lu and X. W. D. Lou, *Angew. Chem. Int. Ed. Engl.,* 2018, **57**, 172-176.
20. X. Wang, L. Yu, B. Y. Guan, S. Song and X. W. D. Lou, *Adv. Mater.*, 2018, DOI: 10.1002/adma.201801211, 1801211.
21. P. He, X. Y. Yu and X. W. Lou, *Angew. Chem. Int. Ed. Engl.*, 2017, **56**, 3897-3900.
22. Z. F. Huang, J. Song, K. Li, M. Tahir, Y. T. Wang, L. Pan, L. Wang, X. Zhang and J. J. Zou, *J. Am. Chem. Soc.*, 2016, **138**, 1359-1365.
23. L. Yu, B. Y. Xia, X. Wang and X. W. Lou, *Adv. Mater.*, 2016, **28**, 92-97.
24. K. Shen, Z. Lei, X. Chen, L. Liu and B. J. S. Chen, *Sci.,* 2018, **359**, 206-210.
25. Y. Yang, J. Liu, Z. W. Fu and D. Qin, *J. Am. Chem. Soc.*, 2014, **136**, 8153-8156.
26. Y. Son, Y. Son, M. Choi, M. Ko, S. Chae, N. Park and J. Cho, *Nano Lett.*, 2015, **15**, 6914-6918.
27. H. B. Wu, B. Y. Xia, L. Yu, X. Y. Yu and X. W. Lou, *Nat Commun.*, 2015, **6**, 6512.
28. J. S. Li, S. Zhang, J. Q. Sha, H. Wang, M. Z. Liu, L. X. Kong and G. D. Liu, *ACS Appl. Mater. Interfaces*, 2018, **10**, 17140-17146.
29. Y. Jin, H. Wang, J. Li, X. Yue, Y. Han, P. K. Shen and Y. Cui, *Adv. Mater.*, 2016, **28**, 3785-3790.
30. H. Li, H. Li, Y. Qiu, S. Liu, J. Fan and X. Guo, *Nano Select*, 2021, **2**, 2148-2158.
31. D. Chen, R. Lu, Z. Pu, J. Zhu, H.-W. Li, F. Liu, S. Hu, X. Luo, J. Wu, Y. Zhao and S. Mu, *Appl. Catal. B Environ.*, 2020, **279**.
32. X. Qin, L. Zhang, G.-L. Xu, S. Zhu, Q. Wang, M. Gu, X. Zhang, C. Sun, P. B. Balbuena, K. Amine and M. Shao, *ACS Catal.*, 2019, **9**, 9614-9621.
33. Y. Liu, S. Liu, Y. Wang, Q. Zhang, L. Gu, S. Zhao, D. Xu, Y. Li, J. Bao and Z. Dai, *J. Am. Chem. Soc.*, 2018, **140**, 2731-2734.
34. R. Zhang, X. Wang, S. Yu, T. Wen, X. Zhu, F. Yang, X. Sun, X. Wang and W. Hu, *Adv. Mater.*, 2017, **29**, 1605502.
35. L. Liao, C. Cheng, H. Zhou, Y. Qi, D. Li, F. Cai, B. Yu, R. Long and F. Yu, *Mater. Today Phys.*, 2022, **22**, 100589.
36. D. Y. Li, L. L. Liao, H. Q. Zhou, Y. Zhao, F. M. Cai, J. S. Zeng, F. Liu, H. Wu, D. S. Tang and F. Yu, *Mater. Today Phys.*, 2021, **16**, 100314.
37. J. Wang, W. Fang, Y. Hu, Y. Zhang, J. Dang, Y. Wu, B. Chen, H. Zhao and Z. Li, *Appl. Catal. B Environ.*, 2021, **298**, 120490.
38. P. Jiang, H. Huang, J. Diao, S. Gong, S. Chen, J. Lu, C. Wang, Z. Sun, G. Xia, K. Yang, Y. Yang, L. Wei and Q. Chen, *Appl. Catal. B Environ.*, 2019, **258**, 117965.